Amplification of *E2F1* has been reported in some cancer cell lines and *E2F1* may be a target for the chromosome 20q amplification.[2] High levels of E2F1 in cancers of the lung, breast, and pancreas correlate with poor clinical outcomes.[2] In contrast, reduced E2F1 expression in colon cancer and bladder cancer correlates with more aggressive malignancy. Paradoxically, E2F1 has been shown to have the ability to induce both cell-cycle progression and programmed cell death, potentially leading to both tumor-promoting and tumor-suppressing effects.[7] Deregulation of E2F1 expression can lead to promotion or inhibition of tumorigenesis, depending on what other oncogenic mutations are present.[2]

B-Myb belongs to the Myb family of transcriptional factors, which include A-Myb and C-Myb.[8] Whereas A-Myb and C-Myb are tissue-specific, B-Myb is expressed ubiquitously. B-Myb plays an important role in the cell cycle and in cell survival.[8,9] *MYBL2*, which encodes B-Myb, is induced by E2F1.[10] B-Myb expression is barely detectable in G0 and is induced at the G1/S transition of the cell cycle.[8] The broad expression of B-Myb in proliferating cells at least in part explains the phenotype of B-Myb knockout mice; that is, death in early embryogenesis.[11]

Herein we examined *E2F1* expression in HCC and explored transcriptional targets of E2F1 that are activated in this type of tumor. Intriguingly, *MYBL2* emerged as a likely downstream target of E2F1. Further, we show that B-Myb protein can activate expression of genes that encode CDC2, cyclin A2, and topoisomerase II α, which are required for cell cycle progression.

METHODS

Cell lines and tumor samples

A TOTAL OF 21 liver cancer cell lines were examined in this study: HCC-derived HLE;[12] HLF;[12] PLC/PRF/5; Li7;[13] Huh7; Hep3B; SNU354;[14] SNU368;[14] SNU387;[14] SNU398;[14] SNU423;[14] SNU449;[14] SNU475;[14] JHH-1;[15] JHH-2;[15] JHH-4;[15] JHH-5;[15] JHH-6;[15] JHH-7;[15] Huh-1;[16] and the hepatoblastoma line HepG2. All cell lines were maintained in Dulbecco's modified Eagle's medium (DMEM) supplemented with 10% fetal bovine serum. We obtained a total of 66 primary HCC tumors from patients undergoing surgery at the Tokyo Medical and Dental University and Kyoto University. Before initiation of the present study, informed consent was obtained in the formal style approved by all relevant ethical committees. Genomic DNA was isolated from each cell line and from primary tumors using the Puregene DNA isolation kit (Gentra, MN, USA). Total RNA could be extracted from 41 of these primary HCCs.

Fluorescence *in situ* hybridization (FISH)

We performed FISH using as a probe the bacterial artificial chromosome (BAC) RP11-73E4, which includes *MYBL2*, as described previously.[4] Briefly, the probe was labeled by nick translation with biotin-16-dUTP (Roche Diagnostics, Germany) and hybridized to metaphase chromosomes. Hybridization signals for biotin-labeled probes were detected with avidin-fluorescein (Roche Diagnostics).

Real-time PCR

We quantified genomic DNA and mRNA by real-time fluorescence detection. Total RNA was obtained using Trizol (Invitrogen, CA, USA). Residual genomic DNA was removed by incubating the RNA samples with RNase-free DNase I (Takara Bio, Japan) prior to reverse transcription (RT)-PCR. Single-stranded complementary DNA (cDNA) was generated using Superscript III Reverse Transcriptase (Invitrogen) following the manufacturer's directions. Real-time quantitative PCR experiments were performed with the LightCycler system using Faststart DNA Master Plus SYBR Green I (Roche Diagnostics) according to the manufacturer's protocol. Primer sequences are listed in supplementary Tables S1 and S2. *GAPDH*[17] and long interspersed nuclear element-1 (LINE-1)[18] were used as endogenous controls for mRNA and genomic DNA levels, respectively.

RNA interference studies

For RNA interference (RNAi), small interfering RNA (siRNA) duplex oligoribonucleotides targeting *E2F1* or *MYBL2*, along with a non-silencing control siRNA which has no significant similarity to any known mammalian gene, were obtained from Qiagen (Japan). The siRNAs were delivered into JHH-5 cells using Hyperfect transfection reagent (Qiagen) according to the manufacturer's instructions. To determine mRNA levels, cells were harvested 48 h after transfection and subjected to real-time quantitative RT-PCR as described above.

Statistical analysis

All statistical analyses were performed using SPSS version 15.0 (SPSS, IL, USA). Either the Wilcoxon signed-rank test or the Mann–Whitney *U*-test was used to compare mRNA levels among tumorous and non-tumorous tissues. Any apparent associations were tested via Pearson's correlation coefficient analysis. χ^2-tests

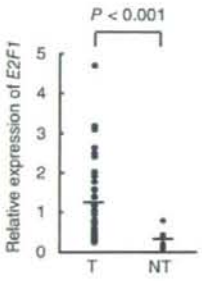

Figure 1 Over-expression of *E2F1* in primary hepatocellular carcinoma (HCC). Relative expression levels of *E2F1* in 41 primary HCC tumors (T) and seven non-tumorous liver tissues (NT) were evaluated by real-time quantitative RT-PCR and normalized to *GAPDH*. Horizontal lines indicate the means of expression levels.

were used to evaluate associations between clinicopathological parameters and the level of *MYBL2* expression. *P* values of <0.05 were considered significant.

RESULTS

Identification of E2F1 downstream genes

WE DETERMINED THE levels of *E2F1* mRNA in 41 primary HCCs and seven non-tumorous liver tissues using real-time quantitative RT-PCR. *E2F1* was significantly over-expressed in HCC tumors as compared to non-tumorous tissues (Mann–Whitney *U*-test, $P < 0.001$; Fig. 1).

To identify genes induced by E2F1 in HCC, we examined ten candidate genes thought to be targets of E2F1: *MYBL2* (which encodes B-Myb); *CDC2* (CDC2/CDK1); *CCNA2* (cyclin A2); *CCNE1* (cyclin E); *MYC* (c-MYC); *DHFR* (dihydrofolate reductase); *TYMS* (thymidylate synthetase); *TK1* (thymidine kinase 1); *RRM1* (ribonucleotide reductase M1); and *PCNA* (proliferating cell nuclear antigen). For this purpose, we knocked down expression of *E2F1* via siRNA. In HCC-derived JHH-5 cells that received siRNA targeting *E2F1*, we observed a decrease in *E2F1* mRNA levels relative to what was observed for cells that received a control siRNA or for untreated cells (Fig. 2A). Following siRNA-mediated knockdown of *E2F1*, we quantified mRNA levels of the ten candidate genes. Knockdown of *E2F1* led to a decrease in expression of *MYBL2*, *CCNE1*, *MYC*, *TK1*, and *RRM1*, but not *CDC2*, *CCNA2*, *DHFR*, *TYMS*, or *PCNA* (Fig. 2A).

We next determined the expression levels of the ten candidate genes in 41 primary HCCs and seven non-tumorous liver tissues. Real-time quantitative RT-PCR analyses revealed that *MYBL2*, *CDC2*, and *CCNA2* were significantly over-expressed in HCC tumors as compared to non-tumor tissues (Fig. 2B). Among the ten candidates, only *MYBL2* was down-regulated following siRNA-mediated knockdown of *E2F1* and significantly over-expressed in primary HCCs. Therefore, we chose to further analyze *MYBL2*, which encodes the transcriptional factor B-Myb.

To further test if over-expression of *MYBL2* correlates with primary HCC tumors, we quantified *MYBL2* expression in paired tumor and non-tumor tissues from an additional 22 patients with HCC. *MYBL2* was significantly over-expressed in 20 (91%) of the tumors as compared to their non-tumorous counterparts (Wilcoxon signed-rank test, $P < 0.001$; Fig. 2C). Further, the expression of *MYBL2* significantly correlated with those of *E2F1* in the 22 primary HCC tumors (Fig. 2D) and in the 21 HCC cell lines (Fig. 2E). Taken together, these observations indicate that *MYBL2* is up-regulated in HCC and is a probable transcriptional target of E2F1.

To clarify the relationship between expression of *MYBL2* and various clinicopathological parameters, we

Figure 2 *MYBL2* is up-regulated in hepatocellular carcinoma (HCC) and is a probable transcriptional target of *E2F1*. (A) siRNA-mediated knockdown of *E2F1* in HCC cell lines. JHH-5 cells were treated with 5 nM siRNA targeting *E2F1* (si*E2F1*) or control siRNA (non-silencing) and harvested 48 h after transfection. Untreated cells were maintained under identical experimental conditions. Relative expression of *E2F1* and its ten putative downstream genes was evaluated by real-time quantitative RT-PCR. Results are presented as the ratio between expression of each gene and a reference gene (*GAPDH*) to correct for variation in the amount of RNA. Relative expression levels were normalized such that for untreated cells, this ratio is 1. (B) Expression of ten putative *E2F1*-downstream genes in 41 primary HCC tumors (T) relative to expression in seven non-tumorous liver tissues (NT). Horizontal lines indicate the means of expression levels. (C) Relative expression of *MYBL2* in paired tumor (T) and non-tumor (NT) tissues from 22 patients with HCC. (D, E) Correlation between expression levels of *E2F1* and *MYBL2* in 22 primary HCC tumors (D) and 21 HCC cell lines (E). Pearson's correlation coefficient analysis revealed that there was a significant correlation between expression levels of the two genes. (□) untreated, (▨) non-silencing, (■) siE2F1.

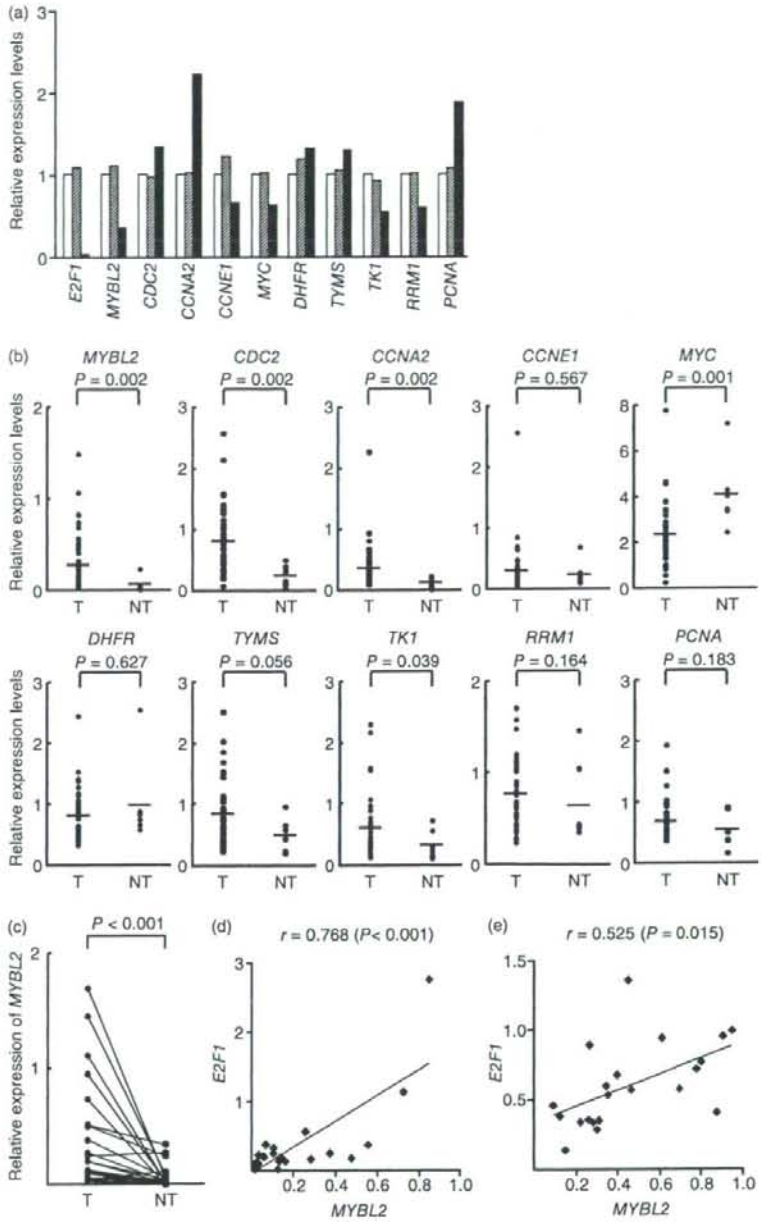

Table 1 Relationship between clinicopathological features and expression levels of *MYBL2* in 37 hepatocellular carcinomas (HCC)

	MYBL2		*P**
	Low (≤ median) (n = 19)	High (> median) (n = 18)	
Age			
<65	6	13	0.013
≥65	13	5	
Sex			
Male	13	14	0.522
Female	6	4	
Tumor size			
<5 cm	8	11	0.248
≥5 cm	11	7	
Tumor differentiation			
Well	3	2	0.403
Moderate	11	14	
Poorly	5	2	
Stage			
I, II, III	16	12	0.214
IV	3	6	
HBV infection status			
Positive	2	6	0.158
Negative	16	10	
Unknown	1	2	
HCV infection status			
Positive	15	11	0.491
Negative	3	5	
Unknown	1	2	
Backgroud liver tissue			
Normal	1	1	0.492
Chronic hepatitis	15	11	
Liver Cirrhosis	1	4	
Unknown	2	2	

*χ^2 test.

next examined the available data from 37 HCC patients, whose tumors were divided into high- and low-expression groups based on where they fell relative to the median of level of *MYBL2* mRNA expression (Table 1). High expression of *MYBL2* was significantly associated with samples from patients less than 65 years old as compared with samples from patients 65 and older. However, we observed no significant link with any other parameter that was examined, including the sex of the patient, the size, degree of differentiation, or stage of the tumor, HBV or HCV infection, or features of non-tumorous liver samples from these patients.

Amplification of *MYBL2* in HCC

Amplification of chromosomal DNA is one of several mechanisms capable of activating genes, a phenomenon that contributes to the development and progression of cancers. *MYBL2* is located at 20q13, where a gain in DNA copy number is frequently observed in various tumors,[19] including HCC.[20] Based on this observation, we decided to determine the *MYBL2* copy number in DNA derived from 21 liver cancer cell lines (20 HCC cells and the hepatoblastoma line HepG2) using real-time quantitative PCR. Copy number changes were counted as gains if the results for a given cell line exceeded the mean plus twice the standard deviation of the levels of *MYBL2* observed in genomic DNA derived from four samples of peripheral blood lymphocytes (i.e. from normal cells). *MYBL2* exhibited copy-number gain in 19 of the 20 lines (Fig. 3A). We then used FISH to more directly test copy-number gain of *MYBL2* in these cell lines. In JHH-5 cells, a representative example, the number of FISH signals was higher than normal (i.e. seven signals were detected in single cells; Fig. 3B). In addition, to ask if *MYBL2* was amplified in primary tumors, we examined 66 primary HCCs for a gain in copy number. Copy-number gain for *MYBL2* was observed in 36 of the 66 tumors (55%; Fig. 3C). These findings suggested that copy-number gain of *MYBL2* acts synergistically with transcriptional activity of E2F1 to upregulate *MYBL2* expression in HCCs.

B-Myb downstream genes

To explore B-Myb-inducible genes in HCC, we analyzed eight genes previously reported to be downstream targets of B-Myb: *CDC2*;[21] *CCNA2*;[22] *TOP2A* (which encodes DNA topoisomerase II α);[23] *FGF4* (fibroblast growth factor 4);[24] *POLA* (DNA polymerase α);[25] *CCND1* (cyclin D1);[21] *CLU* (clusterin/Apo1);[26] and *BCL2* (BCL-2).[27] Of these, *CDC2*, *CCNA2*, *TOP2A*, *FGF4*, *POLA*, and *CCND1* have been implicated in progression of cell cycle, and *CLU* and *BCL2* appear to be involved in anti-apoptotic activity. We knocked down expression of *MYBL2* via siRNA in JHH-5 cells (Fig. 4A). Upon siRNA-mediated knockdown of *MYBL2*, we observed reduced expression of only *CDC2*, *CCNA2*, and *TOP2A* among the eight candidate genes examined (Fig. 4A). These three genes (*CDC2*, *CCNA2*, and *TOP2A*) were significantly over-expressed in 22 primary HCC tumors as compared with their counterpart non-tumorous tissues (Fig. 4B); that is, *CDC2* was over-expressed in 21 HCC tumors (95%); *CCNA2* in 20 (91%); and *TOP2A* in 19 (86%). Moreover, expression levels of *MYBL2*

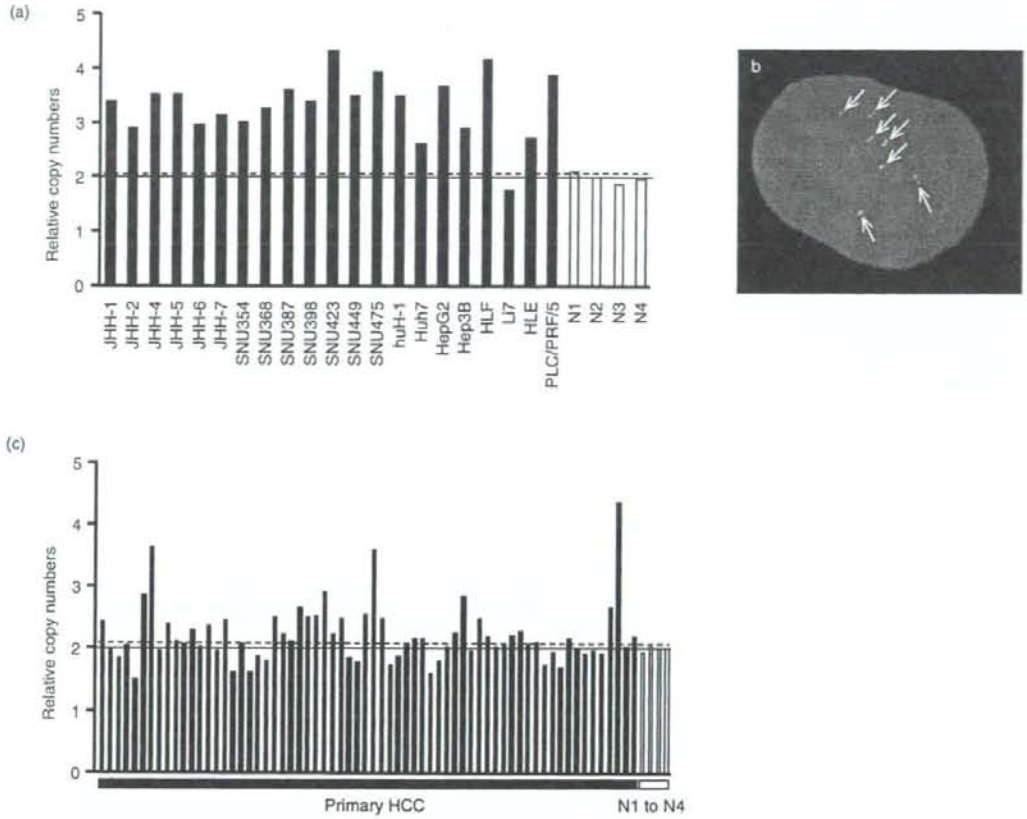

Figure 3 Amplification of *MYBL2* in hepatocellular carcinoma (HCC). (A) Relative copy number of *MYBL2* determined by real-time quantitative PCR in 21 HCC cell lines and normal peripheral lymphocytes (N1 to N4). Results are presented as the ratio between *MYBL2* and a LINE-1 control, and were normalized such that the average ratio in four normal DNAs (N1 to N4) is 2 (solid horizontal line). The mean + 2 × SD of normal lymphocytes (dotted line) was used as the cut-off for a copy-number gain. (B) Representative image of interphase FISH for *MYBL2* in JHH-5 cells. In this case, seven twin-spot FISH signals can be observed. (C) Relative copy number of *MYBL2* in 66 primary HCC tumors determined as in (A). Values were normalized such that the average copy number of *MYBL2* in genomic DNA derived from four normal lymphocytes is 2 (solid horizontal line). The mean + 2 × SD of normal lymphocytes (dotted line) was used as the cut-off for a copy-number gain.

significantly correlated with those of *CDC2*, *CCNA2*, and *TOP2A* in 22 primary HCCs (Fig. 4C). These results suggest that *CDC2*, *CCNA2*, and *TOP2A* are probable transcriptional targets of B-Myb in HCC.

DISCUSSION

IN THE PRESENT study, we examined expression of *E2F1* and candidate E2F1 target genes in primary HCCs. Our results show that both *E2F1* and *MYBL2* are over-expressed in primary HCCs (Figs 1,2B,C) and that there is a significant correlation between expression of *E2F1* and *MYBL2* (Fig. 2D). RNAi-mediated reduction of *E2F1* in HCC-derived cells inhibits expression of *MYBL2* (Fig. 2A). These findings suggest that *MYBL2* may be a transcriptional target of E2F1, which could explain the upregulation of *MYBL2* we observed in HCC. Furthermore, a gain in *MYBL2* copy-number was frequently observed in both HCC cell lines and primary HCC tumors (Fig. 3). Thus, in addition to

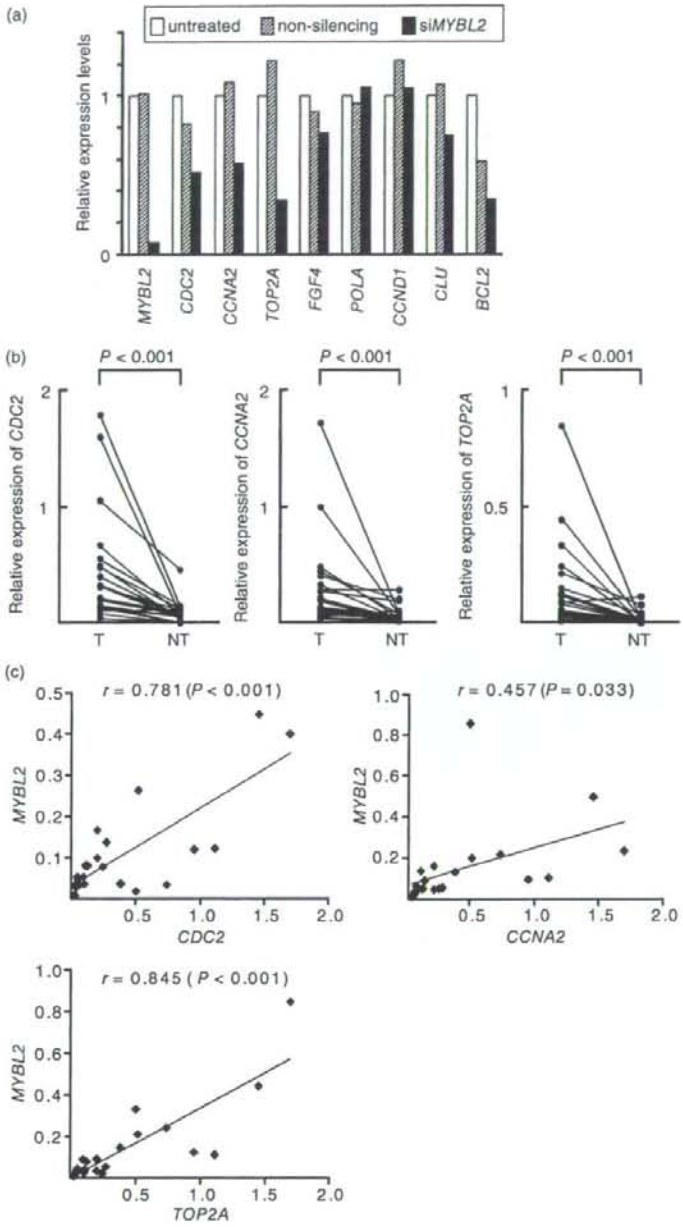

Figure 4 *CDC2*, *CCNA2*, and *TOP2A* are probable transcriptional targets of *MYBL2* in hepatocellular carcinoma (HCC). (A) siRNA-mediated knockdown of *MYBL2* in HCC cell lines. JHH-5 cells were treated with 5 nM siRNA targeting *MYBL2* (si*MYBL2*) or control siRNA (non-silencing), and harvested 48 h after transfection. Untreated cells were maintained under identical experimental conditions. Relative expression of *MYBL2* and putative downstream genes were evaluated by real-time quantitative RT-PCR. Results are presented as the ratio between expression of each gene and a reference (*GAPDH*) to correct for variation in the amount of RNA. Relative expression levels were normalized such that the ratio in untreated cells is 1. (B) Relative expression of *CDC2*, *CCNA2*, and *TOP2A* in paired tumor (T) and non-tumor (NT) tissues from 22 patients as determined by real-time quantitative RT-PCR. (C) Correlation between expression of *MYBL2* and that of *CDC2*, *CCNA2*, or *TOP2A* in 22 primary HCC tumors. Pearson's correlation coefficient analysis revealed that there was a significant correlation between the level of expression of *MYBL2* and that of each of the three genes.

transcriptional activation of *MYBL2* by E2F1, expression of *MYBL2* may also be upregulated in HCC as a result of amplification of the *MYBL2*-containin genomic region in these cells.

Our results are consistent with earlier research. *MYBL2* is frequently amplified in a variety of tumor types, including breast,[28] ovarian,[29] melanoma,[30] and HCC.[31] Moreover, *MYBL2* is amplified and over-expressed in breast cancer cell lines.[32] *MYBL2* is over-expressed in prostate metastases relative to localized tumors.[33] Elevated expression of *MYBL2* is also observed in advanced neuroblastoma and correlates with a poor prognosis.[34] Although the direct role of B-Myb in cancers is not yet fully established, these lines of evidence, together with ours, indicate that B-Myb has oncogenic potential.

We also looked at the relationship between expression levels of *MYBL2* in primary HCCs and clinicopathological parameters (Table 1). With the exception of the age of the patient, no parameter tested, including tumor size, differentiation or stage, correlated with *MYBL2* expression. This may suggest that *MYBL2* is upregulated in early stages of HCC formation.

We next examined transcriptional targets of B-Myb in HCC. Among the eight candidate genes examined, only *CDC2*, *CCNA2*, and *TOP2A* were suppressed at the mRNA level following siRNA-mediated knockdown of *MYBL2* (Fig. 4A). Correspondingly, these three genes are significantly over-expressed in primary HCC tumors (Fig. 4B) and expression of the three genes correlates with *MYBL2* expression (Fig. 4C). These results suggest that *CDC2*, *CCNA2*, and *TOP2A* are downstream targets of B-Myb. Interestingly, Cyclin A2, which is encoded by *CCNA2*, forms a complex with CDC2, whose activity peaks at the G2/M transition of cell cycle, and CDC2-cyclin A2 kinase activity is required to enter M phase. Our results are consistent with the recent findings that B-Myb, together with E2F1, regulates expression of genes required for the G2/M phase of the cell cycle, such as CDC2, cyclin A2, and cyclin B1.[22]

We found that si-RNA-mediated reduction of *E2F1* inhibited expression of *MYBL2*, but not *CCNA2* (Fig. 2A). However, si-RNA-mediated knockdown of *MYBL2* inhibited expression of *CCNA2* (Fig. 4A). It is unclear why reduction of *E2F1* did not lead to a decrease in expression of *CCNA2* through a decrease in the expression of *MYBL2*. There might be a time lag between suppression of *MYBL2* and *CCNA2* expression following si-RNA-mediated knockdown of *E2F1*.

Topoisomerase II α, which is encoded by *TOP2A*, forms breaks in double-stranded DNA, allowing strands to separate during replication. Cyclin A2, CDC2, and topoisomerase II α are all essential for cell cycle progression. Thus, these genes seem reasonable target for B-Myb regulation.

We have shown that *E2F1* is over-expressed in primary HCC tumors and that *MYBL2* expression is also up-regulated in HCCs, suggesting that *MYBL2* is a transcriptional target of E2F1. Frequent amplification of *MYBL2* in HCCs is likely to be an additional mechanism leading to *MYBL2* over-expression. Further, the *CDC2*, *CCNA2*, and *TOP2A* genes may be transcriptional targets of B-Myb. Our results suggest that B-Myb may play an important role in initiation or progression (or both) of HCC and thus, may represent an optimal target for development of novel therapies for this widespread tumor type.

ACKNOWLEDGMENT

THIS WORK WAS supported by Grants-in-Aid for Scientific Research from the Japan Society for the Program of Science (KY).

REFERENCES

1 El-serag HB. Hepatocellular carcinoma: an epidemiologic view. *J Clin Gastroenterol* 2002; 35: S72–8.
2 Johnson DG, Degregori J. Putting the oncogenic and tumor suppressive activities of E2F into context. *Curr Mol Med* 2006; 6: 731–8.

3 DeGregori J, Johnson DG. Distinct and overlapping roles for E2F family members in transcription, proliferation and apoptosis. *Curr Mol Med* 2006; 6: 739–48.
4 Yasui K, Arii S, Zhao C *et al.* TFDP1, CUL4A, and CDC16 identified as targets for amplification at 13q34 in hepatocellular carcinomas. *Hepatology* 2002; 35: 1476–84.
5 Shinomiya T, Mori T, Ariyama Y *et al.* Comparative genomic hybridization of squamous cell carcinoma of the esophagus: the possible involvement of the DP1 gene in the 13q34 amplicon. *Genes Chromosomes Cancer* 1999; 24: 337–44.
6 Yasui K, Okamoto H, Arii S, Inazawa J. Association of over-expressed TFDP1 with progression of hepatocellular carcinomas. *J Hum Genet* 2003; 48: 609–13.
7 Bell LA, Ryan KM. Life and death decisions by E2F-1. *Cell Death Differ* 2004; 11: 137–42.
8 Sala A. B-MY B, a transcription factor implicated in regulating cell cycle, apoptosis and cancer. *Eur J Cancer* 2005; 41: 2479–84.
9 Joaquin M, Watson RJ. Cell cycle regulation by the B-Myb transcription factor. *Cell Mol Life Sci* 2003; 60: 2389–401.
10 DeGregori J, Kowalik T, Nevins JR. Cellular targets for activation by the E2F1 transcription factor include DNA synthesis- and G1/S-regulatory genes. *Mol Cell Biol* 1995; 15: 4215–24.
11 Tanaka Y, Patestos NP, Maekawa T, Ishii S. B-myb is required for inner cell mass formation at an early stage of development. *J Biol Chem* 1999; 274: 28067–70.
12 Dor I, Namba M, Sato J. Establishment and some biological characteristics of human hepatoma cell lines. *Gann* 1975; 66: 385–92.
13 Hirohashi S, Shimosato Y, Kameya T *et al.* Production of alpha-fetoprotein and normal serum proteins by xenotransplanted human hepatomas in relation to their growth and morphology. *Cancer Res* 1979; 39: 1819–28.
14 Park JG, Lee JH, Kang MS *et al.* Characterization of cell lines established from human hepatocellular carcinoma. *Int J Cancer* 1995; 62: 276–82.
15 Fujise K, Nagamori S, Hasumura S *et al.* Integration of hepatitis B virus DNA into cells of six established human hepatocellular carcinoma cell lines. *Hepatogastroenterology* 1990; 37: 457–60.
16 Huh N, Utakoji T. Production of HBs-antigen by two new human hepatoma cell lines and its enhancement by dexamethasone. *Gann* 1981; 72: 178–9.
17 Minamiya Y, Matsuzaki I, Sageshima M *et al.* Expression of tissue factor mRNA and invasion of blood vessels by tumor cells in non-small cell lung cancer. *Surg Today* 2004; 34: 1–5.
18 Zhao X, Li C, Paez JG *et al.* An integrated view of copy number and allelic alterations in the cancer genome using single nucleotide polymorphism arrays. *Cancer Res* 2004; 64: 3060–71.
19 Knuutila S, Björkqvist AM, Autio K *et al.* DNA copy number amplifications in human neoplasms: review of comparative genomic hybridization studies. *Am J Pathol* 2000; 157: 689.
20 Okamoto H, Yasui K, Zhao C, Arii S, Inazawa J. PTK2 and EIF3S3 genes may be amplification targets at 8q23-q24 and are associated with large hepatocellular carcinomas. *Hepatology* 2003; 38: 1242–9.
21 Sala A, Calabretta B. Regulation of BALB/c 3T3 fibroblast proliferation by B-myb is accompanied by selective activation of cdc2 and cyclin D1 expression. *Proc Natl Acad Sci USA* 1992; 89: 10415–19.
22 Zhu W, Giangrande PH, Nevins JR. E2Fs link the control of G1/S and G2/M transcription. *EMBO J* 2004; 23: 4615–26.
23 Brandt TL, Fraser DJ, Leal S, Halandras PM, Kroll AR, Kroll DJ. c-Myb trans-activates the human DNA topoisomerase II alpha gene promoter. *J Biol Chem* 1997; 272: 6278–84.
24 Johnson LR, Johnson TK, Desler M *et al.* Effects of B-Myb on gene transcription: phosphorylation-dependent activity ans acetylation by p300. *J Biol Chem* 2002; 277: 4088–97.
25 Watson RJ, Robinson C, Lam EW. Transcription regulation by murine B-myb is distinct from that by c-myb. *Nucleic Acids Res* 1993; 21: 267–72.
26 Cervellera M, Raschella G, Santilli G *et al.* Direct transactivation of the anti-apoptotic gene apolipoprotein J (clusterin) by B-MYB. *J Biol Chem* 2000; 275: 21055–60.
27 Grassilli E, Salomoni P, Perrotti D, Franceschi C, Calabretta B. Resistance to apoptosis in CTLL-2 cells overexpressing B-Myb is associated with B-Myb-dependent bcl-2 induction. *Cancer Res* 1999; 59: 2451–6.
28 Ginestier C, Cervera N, Finetti P *et al.* Prognosis and gene expression profiling of 20q13-amplified breast cancers. *Clin Cancer Res* 2006; 12: 4533–44.
29 Tanner MM, Grenman S, Koul A *et al.* Frequent amplification of chromosomal region 20q12-q13 in ovarian cancer. *Clin Cancer Res* 2000; 6: 1833–9.
30 Koynova DK, Jordanova ES, Milev AD *et al.* Gene-specific fluorescence in-situ hybridization analysis on tissue microarray to refine the region of chromosome 20q amplification in melanoma. *Melanoma Res* 2007; 17: 37–41.
31 Zondervan PE, Wink J, Alers JC *et al.* Molecular cytogenetic evaluation of virus-associated and non-viral hepatocellular carcinoma: analysis of 26 carcinomas and 12 concurrent dysplasias. *J Pathol* 2000; 192: 207–15.
32 Forozan F, Mahlamäki EH, Monni O *et al.* Comparative genomic hybridization analysis of 38 breast cancer cell lines: a basis for interpreting complementary DNA microarray data. *Cancer Res* 2000; 60: 4519–25.
33 Bar-Shira A, Pinthus JH, Rozovsky U *et al.* Multiple genes in human 20q13 chromosomal region are involved in an advanced prostate cancer xenograft. *Cancer Res* 2002; 62: 6803–7.

34 Raschellà G, Cesi V, Amendola R *et al.* Expression of B-myb in neuroblastoma tumors is a poor prognostic factor independent from MYCN amplification. *Cancer Res* 1999; 59: 3365–8.

SUPPLEMENTARY MATERIAL

THE FOLLOWING SUPPLEMENTARY material is available for this article online:

Table S1. Primer sequences used for RT-PCR assays.

Table S2. Primer sequences used for genomic PCR assays.

This material is available as part of the online article from http://www.blackwell-synergy.com

GENES, CHROMOSOMES & CANCER 48:109–120 (2009)

RESEARCH ARTICLES

ERK5 is a Target for Gene Amplification at 17p11 and Promotes Cell Growth in Hepatocellular Carcinoma by Regulating Mitotic Entry

Keika Zen,[1] Kohichiroh Yasui,[1]* Tomoaki Nakajima,[1] Yoh Zen,[2] Kan Zen,[3] Yasuyuki Gen,[1] Hironori Mitsuyoshi,[1] Masahito Minami,[1] Shoji Mitsufuji,[1] Shinji Tanaka,[4] Yoshito Itoh,[1] Yasuni Nakanuma,[2] Masafumi Taniwaki,[5] Shigeki Arii,[4] Takeshi Okanoue,[1] and Toshikazu Yoshikawa[1]

[1]Molecular Gastroenterology and Hepatology, Graduate School of Medical Science, Kyoto Prefectural University of Medicine, Kyoto, Japan
[2]Department of Human Pathology, Kanazawa University Graduate School of Medicine, Kanazawa, Japan
[3]Division of Cardiovascular Medicine, Omihachiman Community Medical Center, Omihachiman, Japan
[4]Department of Hepato-Biliary-Pancreatic Surgery, Tokyo Medical and Dental University, Tokyo, Japan
[5]Molecular Hematology and Oncology, Graduate School of Medical Science, Kyoto Prefectural University of Medicine, Kyoto, Japan

Using high-density oligonucleotide microarrays, we investigated DNA copy-number aberrations in cell lines derived from hepatocellular carcinomas (HCCs) and detected a novel amplification at 17p11. To identify the target of amplification at 17p11, we defined the extent of the amplicon and examined HCC cell lines for expression of all seven genes in the 750-kb commonly amplified region. Mitogen-activated protein kinase (MAPK) 7, which encodes extracellular-regulated protein kinase (ERK) 5, was overexpressed in cell lines in which the gene was amplified. An increase in *MAPK7* copy number was detected in 35 of 66 primary HCC tumors. Downregulation of *MAPK7* by small interfering RNA suppressed the growth of SNU449 cells, the HCC cell line with the greatest amplification and overexpression of *MAPK7*. ERK5, phosphorylated during the G2/M phases of the cell cycle, regulated entry into mitosis in SNU449 cells. In conclusion, our results suggest that *MAPK7* is likely the target of 17p11 amplification and that the ERK5 protein product of *MAPK7* promotes the growth of HCC cells by regulating mitotic entry.

INTRODUCTION

Hepatocellular carcinoma (HCC) is the fifth most common malignancy in the world and is estimated to cause approximately half a million deaths annually (El-Serag, 2002). Several risk factors for HCC have been reported, including infection with hepatitis B and C viruses, dietary intake of afratoxin, alcohol consumption, and diabetes.

The mitogen-activated protein kinase (MAPK) cascades transmit extracellular signals from cell surface receptors to specific intracellular targets and regulate a wide variety of cellular functions, including cell proliferation, differentiation, and the stress response (Nishimoto and Nishida, 2006). Extracellular stimuli induce sequential activation of MAPK kinase kinase, MAPK kinase, and MAPK. At least four MAPK subfamilies have been identified: extracellular-regulated protein kinase (ERK) 1 and 2, c-Jun-N-terminal kinases, p38, and ERK5 (also know as BMK1). ERK5, which was recently characterized, can be activated by a wide range of growth factors and cellular stresses, including serum, epithelial growth factor, oxidative stress, and hyperosmotic shock (Hayashi and Lee, 2004; Nishimoto and Nishida, 2006; Wang and Tournier, 2006). When stimulated, MAP/ERK kinase kinase 2 and 3 activate MAP/ERK kinase (MEK) 5, a specific kinase for ERK5. Subsequently, MEK5 phosphorylates ERK5, and the activated ERK5 promotes cell proliferation, differentiation, and survival (Hayashi and Lee, 2004; Garaude et al., 2006; Nishimoto and Nishida, 2006; Wang and Tournier, 2006). Some investigators have described the possible involvement of ERK5 in cancers (Esparis-Ogando et al., 2002; Weldon et al., 2002; Mulloy et al., 2003; Carvajal-Vergara et al., 2005; Linnerth et al., 2005).

Additional Supporting Information may be found in the online version of this article.

Supported by: Grants-in-Aid for Scientific Research from the Japan Society for the Program of Science, Grant number: 18390223.

*Correspondence to: Kohichiroh Yasui, Molecular Gastroenterology and Hepatology, Graduate School of Medical Science, Kyoto Prefectural University of Medicine, 465 Kajii-cho, Kamigyo-ku, Kyoto, 602-8566, Japan. E-mail: yasuik@koto.kpu-m.ac.jp

Received 24 May 2008; Accepted 11 September 2008
DOI 10.1002/gcc.20624
Published online 30 October 2008 in Wiley InterScience (www.interscience.wiley.com).

Accumulating evidence suggests that multiple sequential genetic alterations in a cell lineage at the nucleotide and chromosome levels underlie the carcinogenesis of solid tumors. Amplification of chromosomal DNA is one mechanism of activating genes whose overexpression contributes to the development and progression of cancer. Regions of chromosomal amplification in cancer cells frequently harbor oncogenes, such as *MYC* (Little et al., 1983) and *ERBB2* (Di Fiore et al., 1987). Using comparative genomic hybridization (CGH), we have detected novel regions of amplification in a variety of cancer types, including HCC, and we have identified a number of candidate oncogenes from amplicons (Yasui et al., 2001; Yasui et al., 2002; Yokoi et al., 2002; Okamoto et al., 2003; Yokoi et al., 2003). CGH was initially used for genome-wide detection of copy number changes occurring in cancers (Kallioniemi et al., 1992). However, its resolution is limited (5–10 Mb) because it detects segmental copy number changes on metaphase chromosomes.

The recent introduction of high-density oligonucleotide microarrays designed for typing of single nucleotide polymorphisms (SNPs) facilitates high-resolution mapping of chromosomal amplifications, deletions, and loss of heterozygosity (Mei et al., 2000; Bignell et al., 2004; Matsuzaki et al., 2004a,b; Wong et al., 2004; Zhao et al., 2004). The Affymetrix GeneChip Mapping 100K array set contains 116,204 SNP loci with a mean intermarker distance of 23.6 kb, and it enables detailed and genome-wide identification of DNA copy number changes (Matsuzaki et al., 2004a,b; Garraway et al., 2005; Zhao et al., 2005). The newer GeneChip Mapping 500K array set is composed of two arrays, each capable of genotyping an average 250,000 SNPs.

In the work reported here, we investigated DNA copy number aberrations in HCC cell lines using Affymetrix high-density SNP arrays. We identified a novel amplification at 17p11 in HCC cell lines. This region may harbor one or more genes that, when amplified, contribute to carcinogenesis. Within the amplicon, *MAPK7*, which encodes ERK5, emerged as a probable target gene that acts as a driving force for amplification of the region and promotes the growth of HCC cells by regulating entry into mitosis.

MATERIALS AND METHODS

Cell Lines and Tumor Samples

A total of 21 liver cancer cell lines [HCC-derived HLE, HLF (Dor et al., 1975), PLC/PRF/5 (Alexander et al., 1976), Li7 (Hirohashi et al., 1979), Huh7 (Nakabayashi et al., 1982), Hep3B (Aden et al., 1979), SNU354, SNU368, SNU387, SNU398, SNU423, SNU449, SNU475 (Park et al., 1995), JHH-1, JHH-2, JHH-4, JHH-5, JHH-6, JHH-7 (Fujise et al., 1990), Huh-1 (Huh et al., 1981), and the hepatoblastoma line HepG2 (Knowles et al., 1980)] were examined in this study. All cell lines were maintained in Dulbecco's modified Eagle's medium supplemented with 10% fetal bovine serum. We obtained 66 primary HCC tumors for analysis of the DNA copy number of *MAPK7* from patients undergoing surgery at the hospitals of Tokyo Medical and Dental University and Kyoto University, Japan. Genomic DNA was isolated from each cell line and from 66 primary tumors using the Puregene DNA isolation kit (Gentra, Minneapolis, MN). For immunohistochemical studies of ERK5, 43 additional HCC samples were obtained from the Hospital of Kyoto Prefectural University of Medicine, Japan. Before initiation of the present study, informed consent was obtained in the formal style approved by all relevant ethical committees.

SNP Assay

The GeneChip Mapping 100K array set and GeneChip Mapping 250K Sty array (Affymetrix, Santa Clara, CA) were used in this study. Analyses were performed according to the manufacturer's instructions. In brief, 250 ng of genomic DNA was digested with a restriction enzyme (*Xba*I or *Hind*III for the 100K array set and *Sty*I for the 250K Sty array), ligated to an adaptor, and amplified by PCR (Kennedy et al., 2003; Matsuzaki et al., 2004a,b; Zhao et al., 2004). Amplified products were fragmented, labeled by biotinylation, and hybridized to the microarrays. Hybridization was detected by incubation with a streptavidin-phycoerythrin conjugate, followed by scanning of the array, and analysis was performed as described previously (Kennedy et al., 2003; Di et al., 2005). Copy number changes were calculated using the Copy Number Analyzer for Affymetrix GeneChip Mapping Arrays (http://www.genome.umin.jp) (Nannya et al., 2005).

Fluorescence In Situ Hybridization

We performed FISH using the bacterial artificial chromosome (BAC) RP11-73E4 as a probe (Invitrogen, Carlsbad, CA) as described previously (Yasui et al., 2002). The BAC was selected

on the basis of its location according to the database provided by the UCSC (http://genome.ucsc.edu/). Briefly, the probe was labeled by nick translation with biotin-16-dUTP (Roche Diagnostics, Penzberg, Germany) and hybridized to metaphase chromosomes. Hybridization signals for biotin-labeled probes were detected with avidin-fluorescein (Roche Diagnostics).

Real-Time Quantitative PCR

We quantified genomic DNA and mRNA using a real-time fluorescence detection method. Total RNA was obtained using Trizol (Invitrogen). Residual genomic DNA was removed by incubating the RNA samples with RNase-free DNase I (Takara Bio, Shiga, Japan) prior to reverse transcription (RT)-PCR. Single-stranded complementary DNA was generated using superscript III reverse transcriptase (Invitrogen) according to the manufacturer's directions. Real-time quantitative PCR experiments were performed with the LightCycler system using FastStart DNA Master Plus SYBR Green I (Roche Diagnostics) according to the manufacturer's protocol. The primers were as follows: *MAPK7* DNA (forward, 5′-TGCTGACTGGCTCGAAG-3′; reverse, 5′-GGGTCTGAGATGAACCTGC-3′); *MAPK7* mRNA (forward, 5′-TTTGCCTTACTTCCCACCTG-3′; reverse, 5′-CCCATGTCGAAAGACTGGTT-3′); *GRAP* mRNA (forward, 5′-TCGAAGGACAGACTGCACAC-3′; reverse, 5′-AGAAGAGGAGTGTGCCTCCA-3′); *EPN2* mRNA (forward, 5′-TCACCTCACCCACCACTGTA-3′; reverse, 5′-GTGGTCAGCTGCCCTTAGAG-3′); *EPPB9* mRNA (forward, 5′-CTTTGTGTACGGCCAGGACT-3′; reverse, 5′-CGTAGGGGTTGGTGCTTTTA-3′); *MFAP4* mRNA (forward, 5′-GGTGACTCCCTGTCCTACCA-3′; reverse, 5′-TCATCTCAGTGCGTTTGAGG-3′); *ZNF179* mRNA (forward, 5′-ACTGGGCAGAACCAGAGAGA-3′; reverse, 5′-AGGATGCACAGACAGGCTCT-3′); *FLJ10847* mRNA (forward, 5′-AACTCTTGGGCTTCAAGCAA-3′; reverse, 5′-AGGAGGTTGAGGCTGCAGTA -3′). These primers were designed using Primer3 (http://frodo.wi.mit.edu/cgi-bin/primer3/primer3_www.cgi) on the basis of sequence data obtained from the NCBI database (http://www.ncbi.nlm.nih.gov/). *GAPDH* (Minamiya et al., 2004) and long interspersed nuclear element (LINE)-1 (Zhao et al., 2004) were used as endogenous controls for mRNA and genomic DNA levels, respectively.

Immunoblotting

Immunoblots were prepared according to previously reported methods (Yasui et al., 2001). Cell lysates (20 μg protein per sample) were separated by sodium dodecyl sulfate-polyacrylamide gel electrophoresis on 10% acrylamide gels. We obtained the following antibodies from Sigma-Aldrich (Tokyo, Japan): anti-ERK5 polyclonal antibody, anti-phospho-ERK5 (pThr218/pThr220) polyclonal antibody, and anti-β-actin monoclonal antibody. For immunoblotting, we used anti-ERK5, anti-phospho-ERK5, and anti-β-actin at dilutions of 1:500, 1:1000, and 1:5000, respectively. For secondary immunodetection, we used anti-rabbit or anti-mouse Ig (Amersham, Tokyo, Japan) diluted 1:5000. Protein binding was detected using the ECL system (Amersham).

Immunoprecipitation

Cells were lysed with RIPA buffer (10 mM Tris-HCl, pH 7.4, 150 mM NaCl, 1% Triton X-100, 0.1% sodium dodecyl sulfate, 1% sodium deoxycholate, 1 mM phenylmethylsulfonyl fluoride), and incubated on ice for 30 min. The lysate was centrifuged at 14,000 × *g* at 4°C for 15 min. The supernatant was incubated with normal rabbit IgG and protein A-agarose beads (Santa Cruz Biotechnology, Santa Cruz, CA) to decrease nonspecific protein binding. After centrifugation, the supernatant was incubated with anti-ERK5 polyclonal antibody or normal rabbit IgG (control) overnight at 4°C. Protein A-agarose beads were added to the reaction and the mixture was incubated for an additional 1 hr. The precipitates were recovered by a brief centrifugation, followed by four washes with RIPA buffer. Samples were then boiled in electrophoresis sample buffer and separated by electrophoresis as described above (see "Immunoblotting" section).

Immunohistochemical Analysis

Forty-three primary HCCs, consisting of paired tumor and surrounding nontumor tissues, and two HCC cell lines (SNU449 and Li7) were analyzed by anti-ERK5 immunostaining. Immunohistochemical staining was performed on formalin-fixed and paraffin-embedded sections using an anti-ERK5 polyclonal antibody (Sigma-Aldrich) at a 1:200 dilution. An automated tissue immunostainer (Ventana Medical Systems, Tucson, AZ) was used according to the manufacturer's instructions. The staining was developed with 3,3′-

diaminobenzidine tetrahydrochloride, followed by counterstaining with hematoxylin.

Growth Assays and RNA Interference Studies

For cell growth assays viable cells were stained with 0.2% trypan blue and counted with a hemocytometer 24, 48, and 72 hr after transfection. For RNA interference (RNAi) studies, Stealth small interfering RNA (siRNA) duplex oligoribonucleotides targeting *MAPK7* (5′-CCAUGGCAUGAACCCUGCCGAUAUU-3′) and Stealth RNAi negative control duplexes were synthesized by Invitrogen. The siRNAs were delivered into SNU449 cells using Lipofectamine 2000 (Invitrogen) according to the manufacturer's instructions. To determine mRNA levels, cells were harvested 48 hr after transfection and subjected to quantitative RT-PCR as described above.

Cell Cycle Synchronization

SNU449 cells were synchronized at G1/S, early S, or M phases. For G1/S or early S-phase synchronization, cells were incubated in medium containing 2.5 mM thymidine (Sigma Chemical Co., St. Louis, MO) for 24 hr, followed by 12 hr in medium without thymidine, and finally another 12 hr in medium containing 2.5 mM thymidine (double-thymidine block; for G1/S-phase) or 1 μg/ml aphidicolin (early S-phase block). For M phase synchronization, cells were incubated in medium containing 2.5 mM thymidine for 24 hr, followed by 4 hr in medium without thymidine, and finally another 12 hr in medium containing 0.5 μg/ml nocodazole.

Cell Cycle Analysis

SNU449 cells were synchronized at the G1/S-phase boundary by a double-thymidine block as described above. Synchronized cells were released into fresh medium without thymidine and harvested at the indicated time points. These cells were then stained with propidium iodide and analyzed using a FACSCaliber scanner and Cell Quest software (Becton Dickinson Pharmingen, San Diego, CA).

Mitotic Index

Cells were grown in 24-well plates and transfected with Stealth RNAi targeting *MAPK7* or Stealth RNAi negative control duplexes as described above (see "Growth Assays and RNA Interference Studies" section). After 24 hr, cells were synchronized at the G1/S-phase boundary by a double-thymidine block. Synchronized cells were collected, reseeded on glass slides, and incubated for an additional 9 hr in fresh medium without thymidine. Next, the cells were stained with an anti-phospho-histone H3 antibody that specifically detects mitotic cells. Briefly, cells were fixed with 3.7% formaldehyde, permeabilized with 0.25% Triton X-100, and incubated with PBS containing 1% bovine serum albumin. The cells were then treated with a mixture of 4 μg/ml anti-phospho-histone H3 (Ser10)-biotin conjugated antibody (Upstate Biotechnology, Lake Placid, NY) and a 1:100 dilution of streptavidin-fluorescein (Roche Diagnostics) for 1 hr at room temperature, followed by counterstaining with propidium iodide. Positive staining for phospho-histone H3 was quantified by counting stained cells under a fluorescence microscope and dividing by the number of total cells. The mitotic index was scored as the percentage of mitotic cells in a population. On average, 200 cells were scored in three separate areas.

Statistical Analysis

All statistical analyses were performed using SPSS 15.0 software (SPSS Inc., Chicago, IL). Chi-square tests or analysis of variance (ANOVA) were used. P values < 0.05 were considered significant.

RESULTS

Detection of the 17p11 Amplicon in HCC Cell Lines by SNP Array Analysis

We screened for DNA copy number aberrations in 20 HCC cell lines by SNP array analysis. Two of the 20 cell lines, SNU449 and JHH-7, exhibited amplifications at chromosomal band 17p11 (Fig. 1A). In particular, the SNU449 cell line showed a high level of amplification in a narrow region on 17p11. We were able to define the smallest commonly affected region in the 17p11 amplicon as that lying between the positions recognized by the Affymetrix SNP_A-1662618 and SNP_A-1720748 probes (Fig. 1B). This region includes seven known or predicted protein-coding genes, *GRAP*, *EPN2*, *EPPB9*, *MAPK7*, *MFAP4*, *ZNF179*, and *FLJ10847*. The size of the amplicon was estimated to be approximately 750 kb.

To confirm amplification at 17p11 in SNU449 cells, we performed FISH analysis. The probe for

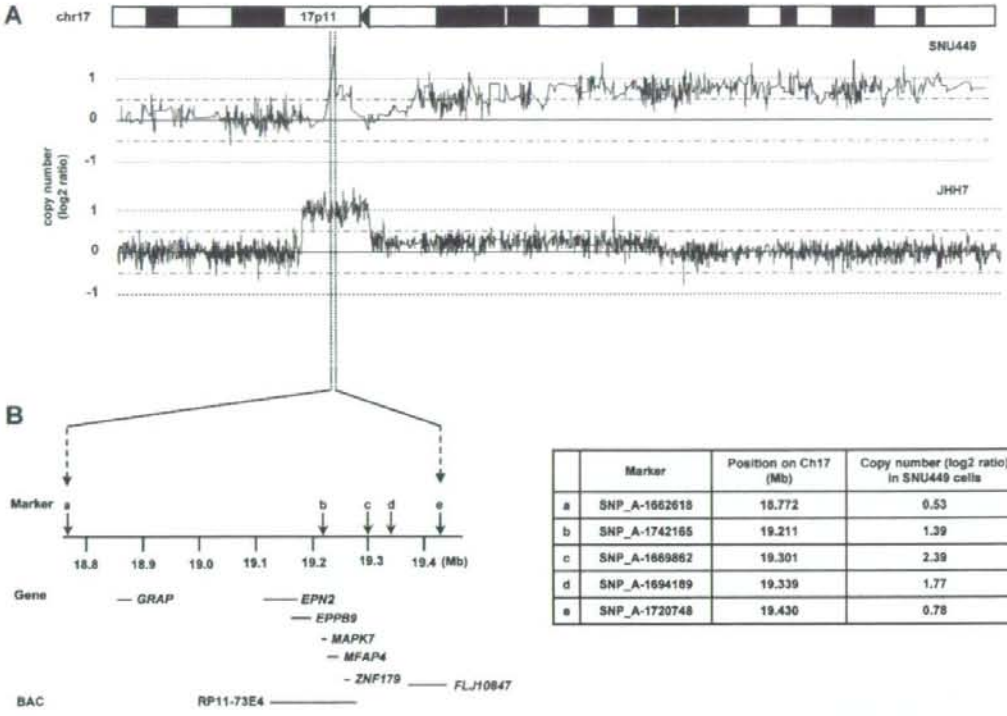

	Marker	Position on Ch17 (Mb)	Copy number (log2 ratio) in SNU449 cells
a	SNP_A-1662618	18.772	0.53
b	SNP_A-1742165	19.211	1.39
c	SNP_A-1669862	19.301	2.39
d	SNP_A-1694189	19.339	1.77
e	SNP_A-1720748	19.430	0.78

Figure 1. Map of the amplicon at 17p11 in two HCC cell lines. A: Copy number profiles for chromosome 17 in SNU449 and JHH-7 cells. Copy number values were determined by SNP 100K and 250K array analyses for SNU449 and JHH-7 cells, respectively. B: The smallest common region of amplification in SNU449 and JHH-7 cells (left). The position of the Affymetrix SNP markers, the seven genes within the amplicon (*GRAP, EPN2, EPPB9, MAPK7, MFAP4, ZNF179,* and *FLJ10847*) and the BAC RP11-73E4 (used as a probe for FISH) are numbered according to the UCSC genome database (http://genome.ucsc.edu/). Detailed copy-number information at positions identified by individual SNP markers over the amplified region in SNU449 cells is shown at right.

these experiments was BAC RP11-73E4, which contains *EPN2*, *EPPB9*, *MAPK7*, *MFAP4*, and *ZNF179* (Fig. 1B). This probe showed an amplified FISH signal on metaphase chromosomes from SNU449 cells (Fig. 2A). To further characterize the relationship between the genes in this chromosomal region and amplifications observed in cancer cells, we analyzed the gene dosage of the *MAPK7* locus by real-time quantitative PCR of DNA from 21 different liver cancer cell lines (20 HCC cell lines and the hepatoblastoma line HepG2). Amplification of *MAPK7* was observed in SNU449 and JHH-7 cells (Fig. 2B). Taken together, the data provide strong evidence that the 17p11 region is amplified in SNU449 and JHH-7 cells.

Analysis of Positional Candidate Genes in HCC Cell Lines

The 17p11 region may harbor one or more genes (henceforth referred to as "target genes") that, when activated by amplification, play a role in carcinogenesis. A common criterion for designating a gene as a putative target is that amplification leads to its overexpression (Collins et al., 1998). Thus, using real-time quantitative PCR, we determined the mRNA levels of all seven genes in the 17p11 amplicon in our panel of 21 liver cancer cell lines. As shown in Fig. 2C, the *EPN2*, *EPPB9*, and *MAPK7* genes were overexpressed in both SNU449 and JHH-7 cells. In several other lines, one or more of these three genes was overexpressed, despite the fact that regional amplification was not observed. These findings suggest that *EPN2*, *EPPB9*, and *MAPK7* are candidate target genes for 17p11 amplification.

Of these three genes, we chose to focus further analysis on *MAPK7*, which encodes ERK5, because ERK5-related proteins have been previously implicated in carcinogenesis (Hayashi and Lee, 2004; Wang and Tournier, 2006), whereas there is little or no evidence linking *EPN2* or

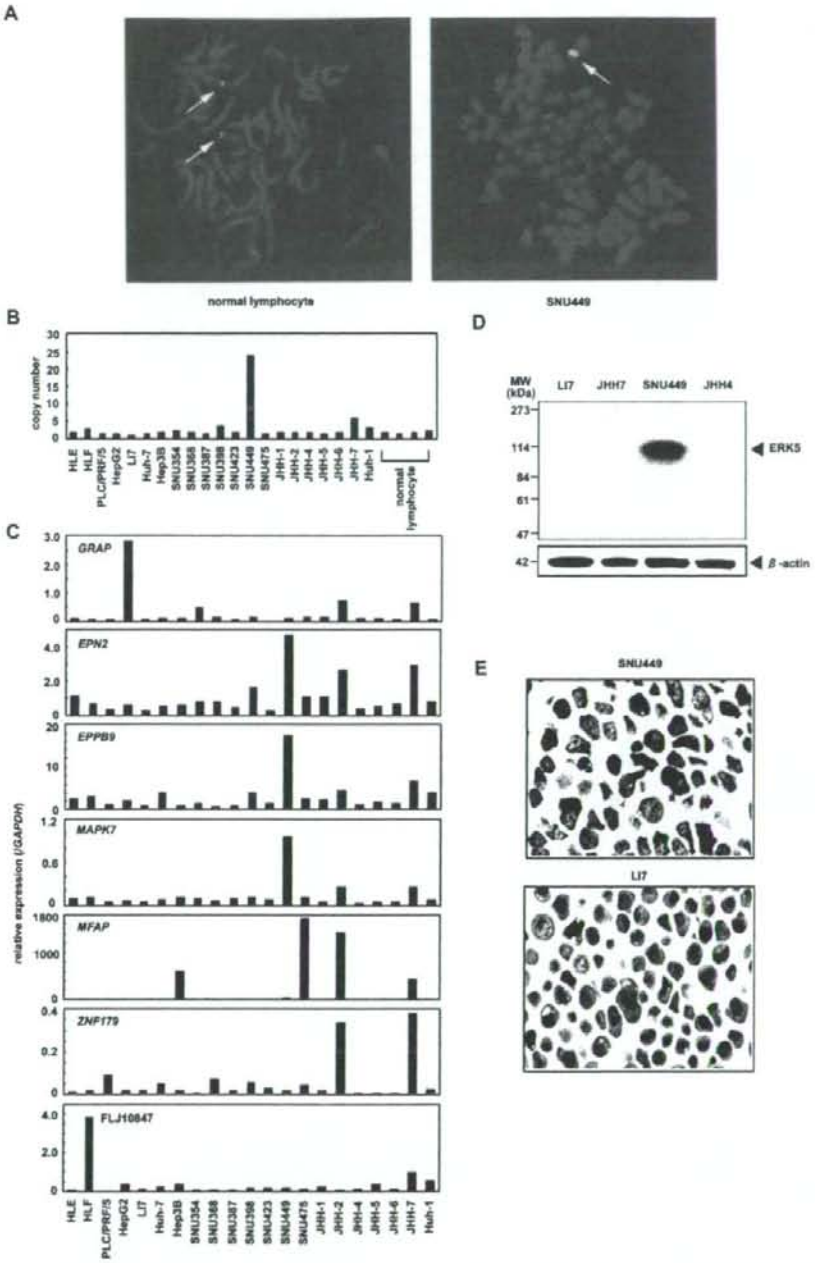

Figure 2. Amplification and overexpression of *MAPK7* in HCC cell lines. (A) Representative images from FISH analysis using a BAC RP11-73E4 probe on metaphase chromosomes from normal lymphocytes and SNU449 cells. While the probe shows a normal signal pattern (2 copies/cell) in normal lymphocytes (arrows, left), it shows an amplified signal in SNU449 cells (arrow, right). (B) Copy number of *MAPK7* in 21 liver cancer cell lines (20 HCC cells and one hepatoblastoma line, HepG2) and four peripheral blood lymphocytes (normal cell controls) as measured by real-time quantitative PCR with reference to a LINE-1 control. Values were normalized such that the average copy number of *MAPK7* in genomic DNA derived from normal lymphocytes is 2. (C) Relative expression levels of the seven genes within the 17p11 amplicon in a panel of 21 liver cancer cell lines as determined by real-time quantitative RT-PCR. The results are presented as the ratio between the expression level of each gene and a reference gene (*GAPDH*) to correct for variation in the amount of RNA. (D) Immunoblot analysis to detect protein levels of ERK5 and β-actin, an internal control, in four HCC cell lines with different *MAPK7* DNA copy numbers (B) and mRNA levels (C). (E) Immunostaining of ERK5 in SNU449 and Li7 cells.

EPPB9 to tumorigenesis. Immunoblot analysis revealed that ERK5 expression is upregulated in SNU449 cells. Indeed, among the HCC cell lines that were tested, SNU449 showed the highest level of both 17p11 amplification and *MAPK7* overexpression (Fig. 2D). Moreover, immunostaining confirmed that the level of ERK5 was elevated in SNU449 cells. ERK5 was strongly expressed in the cytoplasm of SNU449 cells (Fig. 2E). In contrast, ERK5 was weakly expressed in only a few Li7 cells, a HCC cell line that shows neither amplification nor overexpression of *MAPK7* (Fig. 2E).

Copy Number Gain of *MAPK7* in Primary HCC Tumors

To determine whether *MAPK7* is amplified in primary tumors, we examined 66 primary HCCs for copy number gains using real-time quantitative PCR. Copy number changes were counted as gains if the results of the analysis for a given tumor cell type exceeded the mean plus twice the standard deviation (SD) of the levels of *MAPK7* observed in genomic DNA derived from four peripheral blood lymphocyte samples (i.e., normal cells). A copy number gain for *MAPK7* was observed in 35 of the 66 tumors (53%; Fig. 3).

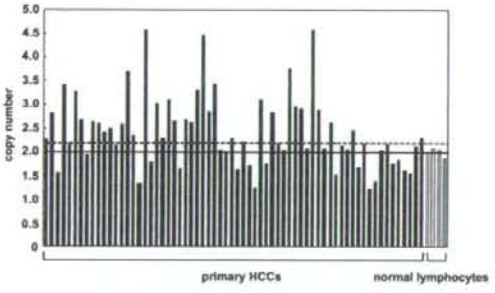

Figure 3. Copy number gain of *MAPK7* in primary HCC tumors. Copy numbers of *MAPK7* in 66 primary HCC tumors and four normal peripheral blood lymphocytes were determined by real-time quantitative PCR with reference to a LINE-1 control. Values were normalized such that the average copy number of *MAPK7* in genomic DNA derived from the normal lymphocytes equals 2 (solid horizontal line). The mean + 2 × SD of normal lymphocytes was used as the cutoff value for copy number gain (dotted line).

Expression of ERK5 in Primary HCCs

We next examined the level of ERK5 in 43 additional primary HCCs, including paired tumor and surrounding nontumor tissues. Immunohistochemical studies revealed that, in nontumor tissues (normal liver, chronic hepatitis, or liver cirrhosis), ERK5 is strongly expressed in bile ducts, bile ductules, and a few small hepatocytes (Fig. 4A). In these cells, ERK5 was present in the cytoplasm. Hepatocytes also contained ERK5, although at a lower level than in bile ducts (Fig. 4A). The staining pattern for ERK5 was almost identical for normal liver, chronic hepatitis, and liver cirrhosis.

This granular cytoplasmic staining for ERK5 was also observed in HCC cancer cells (Fig. 4B). HCC cells containing ERK5 were uniformly distributed in the tumor tissues. The level of ERK5 was elevated in 11 of the 43 tumors compared with the paired nontumor tissues (Figs. 4B and 4C; Supp. Info. Table 1). To clarify the relationship between the level of ERK5 and various clinicopathological parameters, we examined available data from the 43 patients, whose tumors were divided into elevated (T>NT) and not elevated (T≤NT) groups. There was no significant correlation between the level of ERK5 and any parameter examined, including age and gender of the patients; size, stage, and degree of differentiation of the tumor; HBV or HCV infection; and

Figure 4. Representative ERK5 immunostaining of tissues. (A) A nontumorous liver tissue (chronic hepatitis). The level of ERK5 is elevated in the bile duct (large arrow), bile ductules (arrowheads), and a few small hepatocytes (small arrow). (B, C) Paired tumor (B) and nontumor (C) tissues from one HCC patient, wherein the level of ERK5 is elevated in the tumor compared with the counterpart nontumor tissue. Original magnification, ×400.

features of nontumorous liver tissues (Supp. Info. Table 1).

Downregulation of *MAPK7* Inhibits the Growth of HCC Cells

To investigate the effects of *MAPK7* overexpression on HCC cells, we knocked down its expression using RNAi. In SNU449 cells treated with siRNA targeting *MAPK7*, we observed a decrease in *MAPK7* mRNA and ERK5 protein levels relative to that observed for cells receiving a control siRNA or transfection agent alone (Figs. 5A and 5B). The siRNA-mediated downregulation of *MAPK7* suppressed the growth of SNU449 cells at all time points assayed over a 72-hr period (Fig. 5C). These findings suggest that ERK5 promotes the growth of HCC cells.

ERK5 is Phosphorylated During the G2/M Phases of the Cell Cycle

To help elucidate the underlying mechanism by which ERK5 regulates cellular proliferation we investigated the role of ERK5 in cell cycle progression. SNU449 cells were synchronized at G1/S, early S, or M phases of the cell cycle using a double-thymidine, aphidicolin, or nocodazole block, respectively. We determined the levels of total ERK5 and phosphorylated (active) form of ERK5. Immunoblotting did not show a difference in the level of total ERK5 among the three phases of the cell cycle (Fig. 6A). To detect phosphorylated ERK5, total ERK5 was immunoprecipitated from cell lysates using an anti-ERK5 antibody and then analyzed by immunoblotting using an anti-phospho-ERK5 antibody. Phosphorylated ERK5 was more abundant in cells synchronized at the M phase than in asynchronous cells (Fig. 6B).

We next synchronized SNU449 cells at the G1/S boundary using a double-thymidine block and then released the cells from the block. Using flow cytometry, we confirmed the synchrony of the cell cycle and monitored its progression after removal of thymidine (Fig. 6C). There was no difference in the level of total ERK5 during progression of the cell cycle (Fig. 6D). Expression of phosphorylated ERK was maximal 9 hr after release from the block (Fig. 6E), a time when a large proportion of cells were in the G2/M phase (Fig. 6C). Taken together, these observations indicate that ERK5 is phosphorylated during the G2/M phases of the cell cycle.

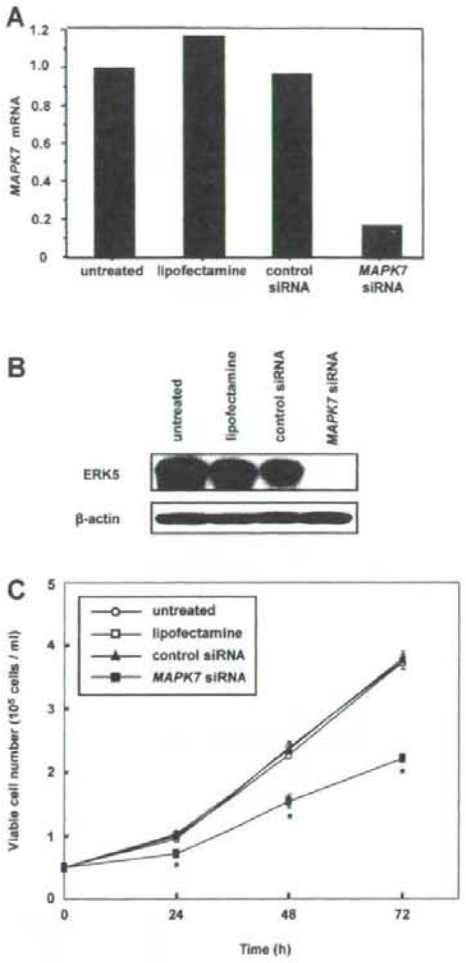

Figure 5. Growth inhibition of SNU449 cells by knockdown of *MAPK7*. A: Relative expression levels of *MAPK7* mRNA as determined by real-time quantitative RT-PCR. SNU449 cells were treated with siRNA targeting *MAPK7*, negative control siRNA, or the transfection agent alone (Lipofectamine), and harvested 48 hr after transfection. Untreated cells were maintained under identical experimental conditions. Results are presented as a ratio between the expression level of *MAPK7* and that of a reference gene (*GAPDH*) to correct for variation in the amount of RNA. Relative expression levels were normalized such that the ratio in untreated cells is 1. B: Levels of ERK5 and β-actin, an internal control, determined by immunoblotting. C: Cell growth was assayed by counting the viable cells at the indicated times after transfection. Each assay was performed in triplicate. Values are represented as the mean ± SD. Differences were analyzed by ANOVA (*$P < 0.01$).

ERK5 Regulates Entry into Mitosis

Our results indicating that ERK5 is activated during the G2/M phases in SNU449 cells suggested that ERK5 may be involved in G2/M progression. To examine whether ERK5 plays a role in mitotic entry, we knocked down *MAPK7*

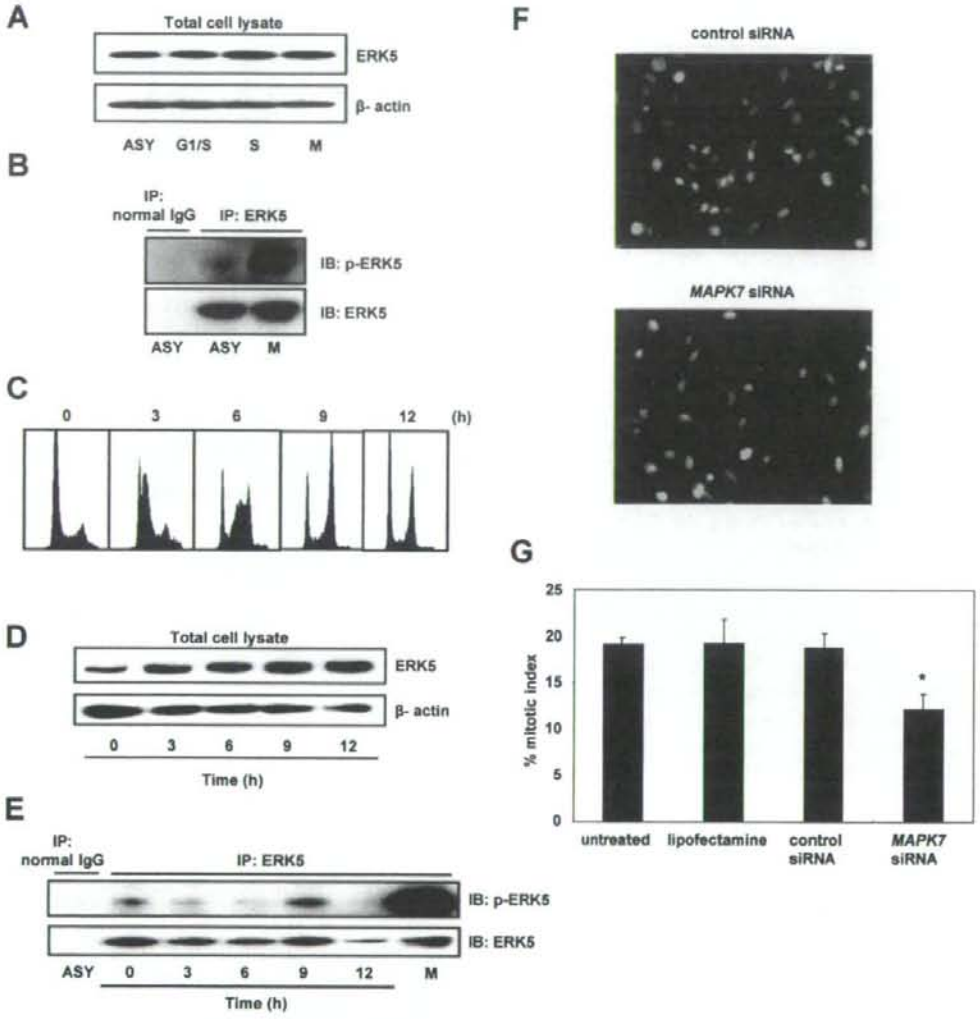

Figure 6. ERK5 is phosphorylated during the G2/M phases of the cell cycle. (A) Immunoblot analysis to detect protein levels of total ERK5 and β-actin, an internal control, in SNU449 cells that were synchronized at the G1/S, early S, or M phases using a double-thymidine, aphidicolin, or nocodazole block, respectively, or were untreated and used as an asynchronous (ASY) population. (B) Levels of phosphorylated ERK5 (p-ERK5). ERK5 was immunoprecipitated (IP) from lysates of SNU449 cells that were synchronized at the M phase (M) or from asynchronous cells (ASY). The samples were split and analyzed by immunoblotting (IB) for p-ERK5 and total ERK5. Normal rabbit immunoglobulin (normal IgG) was used as a negative control for immunoprecipitation. (C) Flow cytometric analysis. SNU449 cells were synchronized to the G1/S boundary using a double-thymidine block. Synchronized cells were released from the block and harvested at the indicated time points. The *X*-axis indicates DNA content and the *Y*-axis indicates the number of cells. (D) Time course of changes in the level of total ERK5 after release from the double-thymidine block. The level of β-actin was used as an internal control. (E) Time course of changes in the level of p-ERK5 after release from the double-thymidine block. ERK5 was immunoprecipitated from lysates of SNU449 cells harvested at the indicated times after release from the double-thymidine block. The samples were split and analyzed by immunoblotting for p-ERK5 and total ERK5. SNU449 cells, synchronized at the M phase with nocodazole, were also examined as described in (A) and (B). Normal rabbit IgG was used as a negative control for immunoprecipitation. (F) Representative images of mitotic cells in an SNU449 cell population that was transfected with *MAPK7*- or control-siRNA. SNU449 cells were treated with siRNA targeting *MAPK7*, negative control siRNA, or the transfection agent alone (Lipofectamine). Untreated cell were maintained under identical conditions. These cells were synchronized at the G1/S boundary using a double-thymidine block. The synchronized cells were released from the block and stained with anti-phospho-histone H3 9 hr after release, a time corresponding to the G2/M phase as shown in (C). Mitotic cells were identified by positive staining for phospho-histone H3 (green). Nuclear DNA was stained with propidium iodide (red). (G) The mitotic index was scored as described in Materials and Methods section. Data are presented as means ± SD (ANOVA: $^*P < 0.05$).

expression using RNAi and assessed its effect on mitosis. SNU449 cells were transfected with siRNA targeting *MAPK7* and synchronized at the G1/S-phase boundary by a double-thymidine block. The synchronized cells were released from the block and harvested 9 hr after release, a time which corresponds to the G2/M phase (Fig. 6C). Finally, harvested cells were stained with anti-phospho-histone H3 antibody, which specifically detects mitotic cells (Fig. 6F). Compared with a control siRNA or transfection agent alone, transfection of *MAPK7* siRNA significantly reduced the mitotic index (Fig. 6G). These findings suggest that ERK5 regulates mitotic entry in the HCC cells.

DISCUSSION

High-density SNP arrays are powerful tools for high-resolution analysis of DNA copy number aberrations in cancers. In the present study, using the Affymetrix GeneChip 100K and 250K SNP arrays we detected a novel amplification in HCC cells at 17p11. We were able to narrow the amplification to a 750-kb region. Notably, the amplification might have been missed using conventional analyses such as CGH. Amplification at 17p11.2-p12 has been detected in high-grade osteosarcoma using CGH (Forus et al., 1995; Tarkkanen et al., 1995). The group of van Dartel et al., (2002) established 17p11.2-p12 amplification profiles by semi-quantitative PCR using 15 microsatellite markers and seven candidate genes to assay amplification in this tumor type. They found that most of the tumors had complex amplification profiles, suggesting that multiple amplification targets, including *MAPK7*, might be present in region 17p11.2-p12. In contrast, we were able to define a smaller common region of amplification at 17p11 in two HCC cells and to determine the expression status of all genes in the amplicon. Three of the seven genes in the amplicon; *EPN2*, *EPPB9*, and *MAPK7*, were always overexpressed in cells that showed amplification in the 17p11 region. Thus, we considered these three genes as candidate targets for amplification. The function of *EPPB9* (B9 protein) is not known, and the protein encoded by *EPN2* (epsin 2) is similar to epsin 1, which plays a putative role in clathrin-mediated endocytosis (Rosenthal et al., 1999). Therefore, we focused on *MAPK7* as a target for the amplification.

Several lines of evidence implicate ERK5, which is encoded by *MAPK7*, in tumorigenesis (Wang and Tournier, 2006): (a) the ERK5 pathway is activated by Ras (English et al., 1999), ErbB (Esparis-Ogando et al., 2002; Yuste et al., 2005), Src (Sun et al., 2003), Cot (Chiariello et al., 2000), Bcr-Abl (Buschbeck et al., 2005), insulin-like growth factor-II (Linnerth et al., 2005), and interleukin-6 (Carvajal-Vergara et al., 2005); (b) ERK5 is involved in the control of breast cancer cell proliferation (Esparis-Ogando et al., 2002); (c) ERK5 mediates a survival signal that confers chemoresistance to breast cancer (Weldon et al., 2002); (d) insulin-like growth factor-II promotes cell survival via the ERK5 pathway in lung cancer cells (Linnerth et al., 2005); (e) the level of ERK5 contributes to the survival of Bcr/Abl-positive leukemic cells (Buschbeck et al., 2005); (f) ERK5 regulates cell proliferation and antiapoptotic responses in multiple myeloma (Carvajal-Vergara et al., 2005); and (g) an elevated level of MEK5, a specific activator of ERK5, is associated with metastasis and a poor prognosis in prostate cancer (Mehta et al., 2003).

The present study is the first to show the status of amplification and expression of *MAPK7* and its functional role in HCC. We found that *MAPK7* is amplified in 35 of 66 HCC tumors (53%). However, we could not determine the copy number of *MAPK7* in the nontumorous counterparts of the samples assayed because these samples were not available. Therefore, we cannot exclude the possibility that copy number polymorphism might influence the results of copy number analysis. We studied the expression of ERK5 using immunohistochemical analysis in primary HCCs and their surrounding nontumorous liver tissues. In nontumorous liver tissues, ERK5 was weakly expressed in the cytoplasm of non-neoplastic hepatocytes. Intriguingly, it was more strongly expressed in bile ducts, bile ductules, and a few small hepatocytes. In HCC tumor tissues, ERK5 was expressed in the cytoplasm of tumor cells. The level of ERK5 was elevated in 11 of 43 HCC tumors compared with their nontumorous counterparts. However, we did not observe a significant link between the level of ERK5 and any clinicopathological parameters. A recent report showed that, in prostate cancer, an increase in ERK5 cytoplasmic signals correlates with advanced disease and that strong nuclear ERK5 localization correlates with poor survival (McCracken et al., 2008).

We examined the functional roles of ERK5 in HCC cells using RNAi. Downregulation of *MAPK7* by siRNA suppressed the growth of

SNU449 cells, which had the greatest amplification and overexpression of *MAPK7* of all of the cell lines tested. These findings suggest that increased levels of ERK5 enhance the growth of HCC cells. Moreover, our results indicate that ERK5 is phosphorylated during the G2/M phases of the cell cycle and that it regulates entry into mitosis, which may explain how it promotes the growth of HCC cells.

Conflicting results have been reported by different investigators regarding the role of ERK5 in cell cycle progression. Some investigators have reported that ERK5 regulates the G1/S transition: expression of a dominant-negative form of ERK5 prevents cells from entering the S-phase of the cell cycle (Kato et al., 1998), and ERK5 can drive cyclin D1 expression (Mulloy et al., 2003). In contrast, Cude et al., (2007) and Gírio et al., (2007) recently reported that ERK5 is activated at the G2/M phases and is required for mitotic entry, findings that agree with our results.

Few molecules have been identified as direct downstream targets of ERK5. The transcriptional factors of the monocyte enhancer factor 2 family are among the best characterized substrates of ERK5. Phosphorylation of monocyte enhancer factor 2C by ERK5 enhances its transcriptional activity and subsequently leads to an increase in c-Jun gene expression (Kato et al., 1997; Wang and Tournier, 2006). A more complete identification of components downstream of ERK5 will be necessary to fully understand the role of ERK5 in carcinogenesis.

In summary, using high-density SNP arrays, we identified *MAPK7* as a probable target for the amplification events at 17p11 in HCCs. Our results suggest that the ERK5 protein product of the *MAPK7* gene plays a role in proliferation of HCC cells by regulating mitotic entry and may therefore be an optimal target for the development of novel therapies for this widespread type of cancer.

REFERENCES

Aden DP, Fogel A, Plotkin S, Damjanov I, Knowles BB. 1979. Controlled synthesis of HBsAg in a differentiated human liver carcinoma-derived cell line. Nature 282:615–616.

Alexander JJ, Bey EM, Geddes EW, Lecatsas G. 1976. Establishment of a continuously growing cell line from primary carcinoma of the liver. S Afr Med J 50:2124–2128.

Bignell GR, Huang J, Greshock J, Watt S, Butler A, West S, Grigorova M, Jones KW, Wei W, Stratton MR, Futreal PA, Weber B, Shapero MH, Wooster R. 2004. High-resolution analysis of DNA copy number using oligonucleotide microarrays. Genome Res 14:287–295.

Buschbeck M, Hofbauer S, Di Croce L, Keri G, Ullrich A. 2005. Abl-kinase-sensitive levels of ERK5 and its intrinsic basal activity contribute to leukaemia cell survival. EMBO Rep 6:63–69.

Carvajal-Vergara X, Tabera S, Montero JC, Esparís-Ogando A, López-Pérez R, Mateo G, Gutiérrez N, Parmo-Cabañas M, Teixidó J, San Miguel JF, Pandiella A. 2005. Multifunctional role of Erk5 in multiple myeloma. Blood 105:4492–4499.

Chiariello M, Marinissen MJ, Gutkind JS. 2000. Multiple mitogen-activated protein kinase signaling pathways connect the cot oncoprotein to the c-jun promoter and to cellular transformation. Mol Cell Biol 20:1747–1758.

Collins C, Rommens JM, Kowbel D, Godfrey T, Tanner M, Hwang SI, Polikoff D, Nonet G, Cochran J, Myambo K, Jay KE, Froula J, Cloutier T, Kuo WL, Yaswen P, Dairkee S, Giovanola J, Hutchinson GB, Isola J, Kallioniemi OP, Palazzolo M, Martin C, Ericsson C, Pinkel D, Albertson D, Li WB, Gray JW. 1998. Positional cloning of ZNF217 and NABC1: Genes amplified at 20q13.2 and overexpressed in breast carcinoma. Proc Natl Acad Sci USA 95:8703–8708.

Cude K, Wang Y, Choi HJ, Hsuan SL, Zhang H, Wang CY, Xia Z. 2007. Regulation of the G2-M cell cycle progression by the ERK5-NFkappaB signaling pathway. J Cell Biol 177:253–264.

Di Fiore PP, Pierce JH, Kraus MH, Segatto O, King CR, Aaronson SA. 1987. erbB-2 is a potent oncogene when overexpressed in NIH/3T3 cells. Science 237:178–182.

Di X, Matsuzaki H, Webster TA, Hubbell E, Liu G, Dong S, Bartell D, Huang J, Chiles R, Yang G, Shen MM, Kulp D, Kennedy GC, Mei R, Jones KW, Cawley S. 2005. Dynamic model based algorithms for screening and genotyping over 100 K SNPs on oligonucleotide microarrays. Bioinformatics 21:1958–1963.

Dor I, Namba M, Sato J. 1975. Establishment and some biological characteristics of human hepatoma cell lines. Gann 66:385–392.

El-Serag HB. 2002. Hepatocellular carcinoma: An epidemiologic view. J Clin Gastroenterol 35:S72–S78.

English JM, Pearson G, Hockenberry T, Shivakumar L, White MA, Cobb MH. 1999. Contribution of the ERK5/MEK5 pathway to Ras/Raf signaling and growth control. J Biol Chem 274:31588–1592.

Esparis-Ogando A, Diaz-Rodriguez E, Montero JC, Yuste L, Crespo P, Pandiella A. 2002. Erk5 participates in neuregulin signal transduction and is constitutively active in breast cancer cells overexpressing ErbB2. Mol Cell Biol 22:270–285.

Forus A, Weghuis DO, Smeets D, Fodstad O, Myklebost O, Geurts van Kessel A. 1995. Comparative genomic hybridization analysis of human sarcomas. II. Identification of novel amplicons at 6p and 17p in osteosarcomas. Genes Chromosomes Cancer 14:15–21.

Fujise K, Nagamori S, Hasumura S, Homma S, Sujino H, Matsuura T, Shimizu K, Niiya M, Kameda H, Fujita K. 1990. Integration of hepatitis B virus DNA into cells of six established human hepatocellular carcinoma cell lines. Hepatogastroenterology 37:457–460.

Garaude J, Cherni S, Kaminski S, Delepine E, Chable-Bessia C, Benkirane M, Borges J, Pandiella A, Iñiguez MA, Fresno M, Hipskind RA, Villalba M. 2006. ERK5 activates NF-kappaB in leukemic T cells and is essential for their growth in vivo. J Immunol 177:7607–7617.

Garraway LA, Widlund HR, Rubin MA, Getz G, Berger AJ, Ramaswamy S, Beroukhim R, Milner DA, Granter SR, Du J, Lee C, Wagner SN, Li C, Golub TR, Rimm DL, Meyerson ML, Fisher DE, Sellers WR. 2005. Integrative genomic analyses identify MITF as a lineage survival oncogene amplified in malignant melanoma. Nature 436:117–122.

Gírio A, Montero JC, Pandiella A, Chatterjee S. 2007. Erk5 is activated and acts as a survival factor in mitosis. Cell Signal 19:1964–1972.

Hayashi M, Lee JD. 2004. Role of the BMK1/ERK5 signaling pathway: Lessons from knockout mice. J Mol Med 82:800–808.

Hirohashi S, Shimosato Y, Kameya T, Koide T, Mukojima T, Taguchi Y, Kageyama K. 1979. Production of -fetoprotein and normal serum proteins by xenotransplanted human hepatomas in relation to their growth and morphology. Cancer Res 39: 1819–1828.

Huh N, Utakoji T. 1981. Production of HBs-antigen by two new human hepatoma cell lines and its enhancement by dexamethasone. Gann 72:178–179.

Kallioniemi A, Kallioniemi OP, Sudar D, Rutovitz D, Gray JW, Waldman F, Pinkel D. 1992. Comparative genomic hybridization for molecular cytogenetic analysis of solid tumors. Science 258:818–821.